Electronic correlation induced expansion of Fermi pockets in δ-plutonium

Roxanne M. Tutchton,[1,*] Wei-ting Chiu,[2] R. C. Albers,[1] G. Kotliar,[3] and Jian-Xin Zhu[1,4,†]

[1]*Theoretical Division, Los Alamos National Laboratory, Los Alamos, New Mexico 87545, USA*
[2]*Department of Physics, University of California, Davis, California 95616, USA*
[3]*Department of Physics and Astronomy, Rutgers University, Piscataway, New Jersey 08854, USA*
[4]*Center for Integrated Nanotechnologies, Los Alamos National Laboratory, Los Alamos, New Mexico 87545, USA*

(Received 7 January 2020; revised manuscript received 14 April 2020; accepted 26 May 2020; published 23 June 2020)

Plutonium is a critically important material as the behavior of its $5f$ electrons stands midway between the metalliclike itinerant character of the light actinides and localized atomic-core-like character of the heavy actinides. The δ phase of plutonium (δ-Pu), whereas still itinerant, has a large coherent Kondo peak and strong electronic correlations coming from its near-localized character. Using sophisticated Gutzwiller wave function and dynamical mean-field theory correlated theories, we study the Fermi surface and associated mass renormalizations of δ-Pu together with calculations of the de Haas–van Alphen frequencies. We find a large ($\sim$200%) correlation induced volume expansion in both the hole and the electron pockets of the Fermi surface in addition to an intermediate mass enhancement. All of the correlated electron theories predict, approximately, the same hole pocket placement in the Brillouin zone, which is different from that obtained in conventional density-functional band-structure theory, whereas the electron pockets from all theories are in, roughly, the same place.

DOI: 10.1103/PhysRevB.101.245156

I. INTRODUCTION

With six allotropic crystal phases at ambient pressure, plutonium (Pu) is one of the most complex elemental solids in the periodic table. Much of its exotic behavior is driven by a large anisotropy natural in its f-electron bonding whose strength is, in turn, tuned by strong electronic correlations, which arises from its $5f$-electron behavior standing midway between the metalliclike itinerant character of the light actinides and the localized atomic-core-like character of the heavy actinides. In addition, these correlations are highly temperature dependent and give rise to a strong atomic volume dependence for the different phases. In particular, the 25% volume expansion between the α and the δ phases gives rise to exotic physics that has appealed to experimentalists and theorists for decades [1–9]. Consequently, the f electrons in the δ phase of plutonium (δ-Pu) appear to exhibit a complex combination of localized and itinerant characteristics making the local moments and their impact on the electronic structure difficult to model [2,10–12].

The magnetic behavior in Pu associated with this $5f$-electron duality has long been a puzzle in the condensed-matter and materials physics community [13–16] since strongly localized electrons typically exhibit some form of magnetism. No long-range magnetic ordering has been observed for any phase of Pu [5,6,8,15]. However, theoretical calculations performed by using density functional theory (DFT), within either the local-density approximation (LDA) or generalized gradient approximation (GGA), cannot reproduce the characteristic volume expansion for δ-Pu unless spin and/or orbital polarization are included [8,17–23]. The LDA $+U$ and GGA $+U$ methods with a large Hubbard-U Coulomb parameter usually favor a magnetic ordering. A recent study [24] based on the GGA $+U$ method implemented in a projector augmented-wave code [25] shows that a weaker Coulomb interaction (i.e., $U \approx 1$ eV) can accurately reproduce the volume phases of Pu without the addition of spin or orbital polarization. It has long been believed that the level of electronic correlation in these approaches were inadequate, and, indeed, strongly correlated electron theoretical methods have recently shown very promising results. By modeling the competition between the on-site Coulomb repulsion among localized f electrons and their hybridization with the itinerant electrons in a quantum impurity fashion, dynamical mean-field theory (DMFT) is able to describe the single-particle excitation properties of δ-Pu in good agreement with photoemission spectroscopy measurements [2,3,26] as well as to predict the valence fluctuations validated by inelastic neutron spectroscopy [12,27]. Another strongly correlated electron theoretical approach uses the Gutzwiller wave-function approximation (GutzA) [28–30], which has been used to successfully calculate the volume dependence in Pu phases without the addition of artificial orbital polarization [29,31]. The combination of LDA (or GGA) and GutzA has the same mathematical structure as LDA combined with DMFT [5] with the difference that the GutzA assumes infinite quasiparticle lifetimes, which is equivalent to neglecting the incoherent component of the electrons. This makes the GutzA method less accurate for calculating strong correlation effects than DMFT. However, it has the important

*rtutchton@lanl.gov
†jxzhu@lanl.gov

compensating advantage of being significantly less computationally demanding [29].

Recently, an attempt has been made to bring magnetism back into the models with the "disordered local moment" [32], involving a static DFT model, which would lead to a Curie behavior for the susceptibility in contradiction to experimental data. The contrasting picture is the "valence fluctuation" [12] (dynamical) model using the DMFT approach described above. The static model describes the orbitals as individual localized magnetic moments that are spatially and temporally disordered such that any long-range magnetic ordering is obscured by averaging over time. The dynamical model proposes a quantum entanglement between the localized magnetic moments and the itinerant conduction electrons, resulting in valence fluctuations that effectively screen the magnetic ordering below the Kondo temperature T_K of the material [12].

In an effort to determine the validity of these theoretical models, previous studies of Pu allotropes have focused on reproducing the volume expansion and bulk modulus of δ-Pu [2,8,29,31,33–37]. This paper strives to fill a gap in the understanding of the momentum space electronic behavior through a direct examination of strong correlation effects. We accomplish this by probing the Fermi surface topology of δ-Pu using the de Haas–van Alphen (dHvA) effect present in metallic systems [38–40], and comparing results for several theoretical methods including DFT within the GGA, the GGA + U (where U is the Hubbard parameter defining the strength of a static Coulomb interaction), the Gutzwiller approximation (GGA + GutzA), and the dynamical mean-field theory (GGA + DMFT). The most striking result includes the discovery of strong correlation induced expansion of compensated electron and hole pockets as well as the relocation of hole pockets.

II. THEORETICAL METHODS

The δ-Pu Fermi-surface topologies were obtained using four electronic structure methods for comparison.

Density functional theory calculations. Our starting point is conventional DFT in the GGA as implemented in the full-potential linearized augmented plane-wave (FP-LAPW) method of WIEN2K [41]. Relativistic spin-orbit coupling effects were included by using a k-point grid of $15 \times 15 \times 15$, a muffin-tin radius of $2.50a_0$, where a_0 is the Bohr radius and a lattice constant $a = 4.637$ Å [42]. These parameters were used for the basis of each calculation method. We note that the GGA normally gives equilibrium volumes a few percent larger than the LDA. When it is combined with the many-body approaches, the equilibrium volume can be overestimated with a large Coulomb interaction when compared with experimental lattice parameters. Here, we choose to use a fixed experimental lattice constant so that the electronic structure properties from different methods can be compared on the same footing. We do not anticipate the use of LDA-based methods will change the results qualitatively.

GGA + U calculations. GGA + U calculations were performed for nonmagnetic δ-Pu using the same parameters and exchange-correlation functional as those used in the DFT method. The Hubbard parameter for the on-site Coulomb interaction strength was tested for values up to $U = 4.5$ eV with an exchange-site parameter of $J = 0.512$ eV, which has been shown to reproduce characteristics of δ-Pu consistent with atomic spectral data [5]. The full electronic structure study for $U = 0$ to 4.5 eV (with $J = 0.512$ eV for $U > 0$) is available in the Supplemental Material (SM) document [43]. In addition to the nonmagnetic cases, ferromagnetic and antiferromagnetic long-range magnetic-ordering cases were explored using the GGA and GGA + U methods. The results can be found in the SM document [43]. These cases were included purely for comparison as there has been no experimental evidence of long-range magnetic ordering detected in any phase of Pu.

Gutzwiller approximation calculations. Similar calculations were performed for paramagnetic δ-Pu using the Gutzwiller approximation method implemented in the CYGUTZ code [29,30]. This method is built upon a FP-LAPW-based DFT [41] calculation and implements a combination of the slave-boson Gutzwiller wave-function method (GutzA) to account for strong electronic correlation. The Coulomb interaction strength was tested at values up to $U = 4.5$ eV to facilitate comparison to the GGA + U and GGA + DMFT (details below) calculations. The electronic structures for $U = 0$ to 4.5 eV (with $J = 0.512$ eV for $U > 0$) is also included in the SM document [43].

Dynamical mean-field theory calculations. GGA + DMFT calculations were also performed for paramagnetic δ-Pu. As in the case of the GGA + U and GGA + GutzA methods, this method uses the FP-LAPW implementation of WIEN2K [41] as its basis. The DMFT calculation implements a strong-coupling version of the continuous-time quantum Monte-Carlo method [26,44,45] in order to explicitly consider the on-site Coulomb interactions with strength $U = 4.5$ and $J = 0.512$ eV. The remaining Slater integrals $F^2 = 6.1$, $F^4 = 4.1$, and $F^6 = 3.0$ eV were calculated using Cowan's atomic-structure code [46] and reduced by 30% to account for screening. Calculations were performed at temperatures of $T = 116$ and $T = 1160$ K. In order to compare the DMFT results to those of the other methods for which $T = 0$ K, the Fermi-surface data were extrapolated from the $T = 0.01$-eV calculation where the sensitivity of the electronic self-energy is negligible. The Fermi energy was then shifted to maintain the conservation of total number of electrons consistent with $T \to 0$ eV.

De Haas–van Alphen calculations. Analysis of the Fermi surfaces from each of the above methods was performed using numerical calculations of the dHvA effect as implemented by Rourke and Julian [39]. By applying a magnetic field to the system, oscillations in the magnetic susceptibility can be determined from the changes in the number of occupied Landau levels as a function of the reciprocal magnetic-field $1/\mathbf{B}$ [39,47]. Then, the dHvA frequency can be expressed as

$$f_i = \frac{1}{\Delta(1/B)} = \frac{\hbar}{2\pi e} A_i, \tag{1}$$

where e is the elementary charge of an electron and A_i is the extremal cross-sectional area of the ith branch of the Fermi surface on a plane perpendicular to $\mathbf{B}$. The effective carrier mass averaged around the extremal cyclotron orbits is also

TABLE I. The dHvA and volume data for Fermi-surface calculations at zero temperature. Frequencies are given in kilotesla (kT), and corresponding effective masses are in units of electron mass (m_e). Reciprocal occupied (electron bands 17 and 18) and unoccupied (hole bands 15 and 16) Fermi-surface volumes are given in units of $Å^{-3}$. Calculations for δ-Pu performed with DFT, the GGA + U, GGA + GutzA, and GGA + DMFT are compared. All measurements were taken for a magnetic field parallel to the z axis ($\mathbf{B} \parallel z$). The results for $T = 0$ K were extrapolated from the GGA + DMFT calculation at $T = 116$ K where the sensitivity of electronic self-energy to temperature is negligible since this temperature is already far below the coherence temperature [27]. The Fermi energy was shifted by −3.36 meV to maintain the conservation of the number of electrons as $T \to 0$ K.

	DFT			GGA + U			GGA + GutzA			GGA + DMFT		
Band	f	m^*	V_{FS}	f	m^*	V_{FS}	f	m^*	V_{FS}	f	m^*	V_{FS}
15 and 16	1.74	3.19	0.31	10.2	2.35	1.02	3.12	2.00	0.91	3.07	1.84	0.95
17 and 18	2.87	5.32	0.31	6.65	1.54	1.02	6.27	2.48	0.91	6.18	2.17	0.95

determined from

$$m^* = \frac{\hbar^2}{2\pi e} \left. \frac{\partial A}{\partial E} \right|_{E=E_F}, \tag{2}$$

where m^* is in units of the electron mass m_e. The results of the dHvA analysis (Table I) are to be compared against magnetic quantum oscillation measurements. We anticipate that such measurements will aid in determining the correct model to describe the physical properties of Pu.

III. RESULTS

A. Electronic structure

The first of the theoretical methods we explored was the standard DFT GGA calculation, which does not explicitly incorporate electronic correlation beyond a simple local exchange-correlation function. The electronic band structure and density of states (DOS) calculated using this method are shown in Fig. 1(a) with the high-symmetry momentum path illustrated in Fig. 2, and the Fermi-surface calculations are given in Fig. 3(a). This calculation is the baseline for the other three methods, each of which adds additional correlation effects using increasingly sophisticated techniques. The GGA + U method applies a static Coulomb interaction to the system within the Kohn-Sham formalism. The GGA + GutzA uses an auxiliary particle theory, whereas assuming infinite quasiparticle lifetimes. The GGA + DMFT is the most sophisticated and computationally demanding method for calculating electronic structure with strong-correlation effects. The resulting band structure for each method is shown in Fig. 1 along with its accompanying DOS. It should be noted that the structure in the DOS for the GGA + DMFT is greatly washed out relative to the other three methods. This is due to quasiparticle lifetime effects naturally included in the GGA + DMFT, whereas the other three methods have sharp (infinite lifetime) quasiparticle states.

The effects of electronic correlation on the quasiparticle band structure is to shift and/or renormalize (distort) the energy bands. The addition of a static Coulomb parameter with the GGA + U [Fig. 1(b)] results in a large shift of the conduction bands just above the Fermi energy and a distortion of the upper valence bands with respect to the GGA results [Fig. 1(a)]. The GGA + U DOS also shows a distinct splitting of the $5f$-electron subshells $j = 5/2$ and $j = 7/2$ with the $j = 5/2$ electron character mainly just below the Fermi energy and the $j = 7/2$ electron character between about 4 to 6 eV for $U = 4.5$ eV. We note that because there is no spin polarization in the present GGA + U calculations (for the purpose of quenching magnetism), the Kramers double degeneracy is restored. Since the Pu-$5f$ shell is partially occupied ($n_f \sim 5$), the $j = 5/2$ subshell must be pulled toward the Fermi energy, and the unoccupied bands are pushed away from the Fermi energy with an increased Hubbard U. The DOS calculated with the GGA + GutzA shows a similar but less dramatic splitting of $5f$ subshells (in part, due to spin-orbit coupling) [Fig. 1(c)]. The corresponding band dispersion indicates a concentration of $5f$ electrons from the $j = 5/2$ subshell around the Fermi energy. There is also an upward shift of the conduction bands and accompanying renormalizations around the Fermi energy as compared to the GGA calculation of Fig. 1(a). This results in flattening of the bands around the X point with increased slopes to the right and left of the flat region. The flattening of the bands in this region is more pronounced than the similar feature in the GGA + U band dispersion [Fig. 1(b)], whereas the shift and resulting slope increase is much more prevalent in the GGA + U method. The band dispersions calculated using the GGA + DMFT [Fig. 1(d)] show, by far, the largest band renormalization of f electrons around the Fermi energy, which is evident from the peak in the DOS (the Kondo peak). This feature is associated with the flattening of the top valence bands and bottom conduction bands around the Fermi energy. Comparing the GGA + GutzA and GGA + DMFT to the GGA + U band structures, we find that the static approach of the GGA + U method does not include the type of band flattening or renormalization of the f-electron bands expected from strong electronic correlations.

B. Fermi-surface topology

We have further explored the behavior of the electronic structure around the Fermi energy through an analysis of the Fermi surfaces shown in Fig. 3 along with sections of the band structure around the Fermi energy. The Brillouin zone (BZ) and high-symmetry paths used in Fig. 1 are displayed in Fig. 2. At first glance, there is a qualitative similarity between the Fermi surfaces from each of the calculation methods. A notable difference in the GGA results is the location of the hole bands (Nos. 15 and 16) intersection with the Fermi energy. The band structures that include some form of correlation effect show the hole pocket occurring between the L

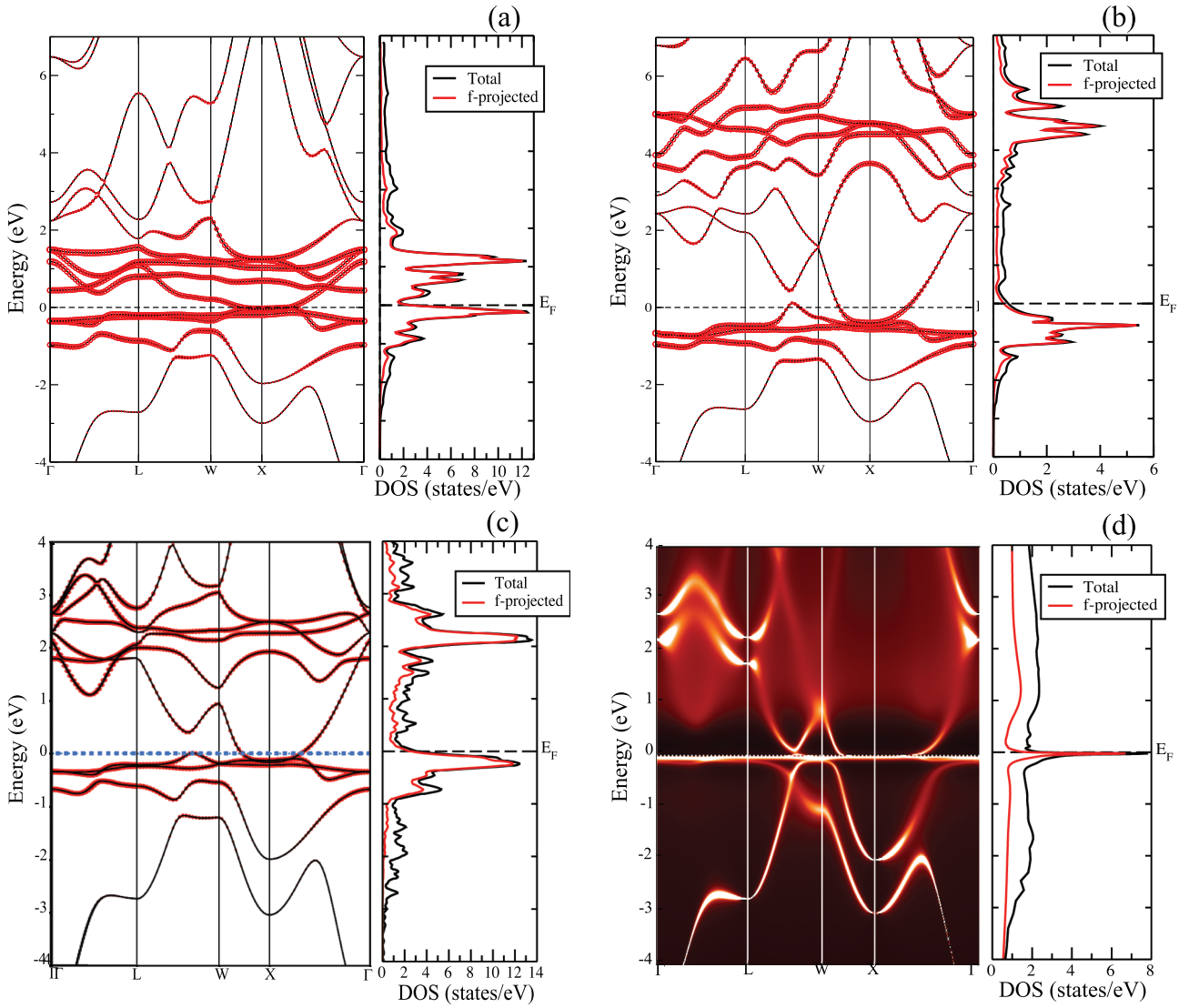

FIG. 1. The electronic band structures and DOS for (a) nonmagnetic δ-Pu calculated using the GGA with no explicit electron-electron correlation, (b) nonmagnetic δ-Pu calculated with the constrained GGA + U for $U = 4.5$ and $J = 0.512$ eV, (c) paramagnetic δ-Pu calculated using the GGA + GutzA for $U = 4.5$ and $J = 0.512$ eV, and (d) paramagnetic δ-Pu calculated using the GGA + DMFT for $U = 4.5$ and $J = 0.512$ eV. The thick red bands indicate the f-electron occupations, and the red curves on the DOS show the f-projected densities. The path that the band dispersions take through the reciprocal space is shown in Fig. 2. Note that whereas the band-structure scales are all the same (between -4 and $+4$ eV) that the DOS scales have different maxima, which should be taken into account when comparing the effects of correlation on the DOS of the four different methods. We have changed the scales to best show the structure in the DOS of each method.

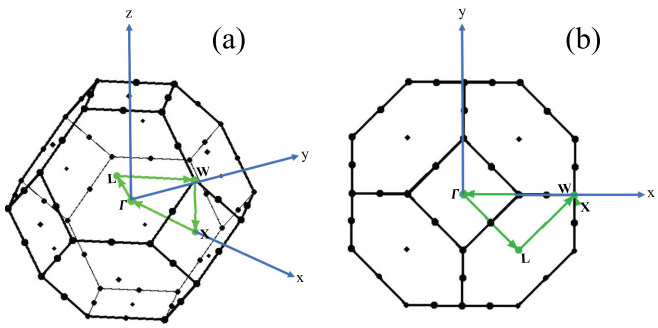

FIG. 2. The high-symmetry path through the first Brillouin zone used for the band-structure calculations goes from $\Gamma \rightarrow L \rightarrow W \rightarrow X \rightarrow \Gamma$.

and the W high-symmetry points, whereas the GGA method has the hole pocket between the X and the Γ points. The rough position of the electron pockets seems unchanged between the GGA and the more correlated electron methods.

We also find differences in dHvA frequencies f_i, which are related to the area of the Fermi surface by the expression $f_i = 1/\Delta(\frac{1}{\mathbf{B}}) = \hbar A_i/2\pi e$, where e is the elementary charge of an electron and A_i is the extremal cross-sectional area of the ith branch of the Fermi surface on a plane perpendicular to the applied magnetic-field $\mathbf{B}$. These frequencies are denoted by the red lines around the isosurfaces in Fig. 3 as well as listed in Table I. In this case, we have calculated the extremal frequencies using a simulated external magnetic field parallel to the Cartesian z axis as indicated in Fig. 2. A full analysis

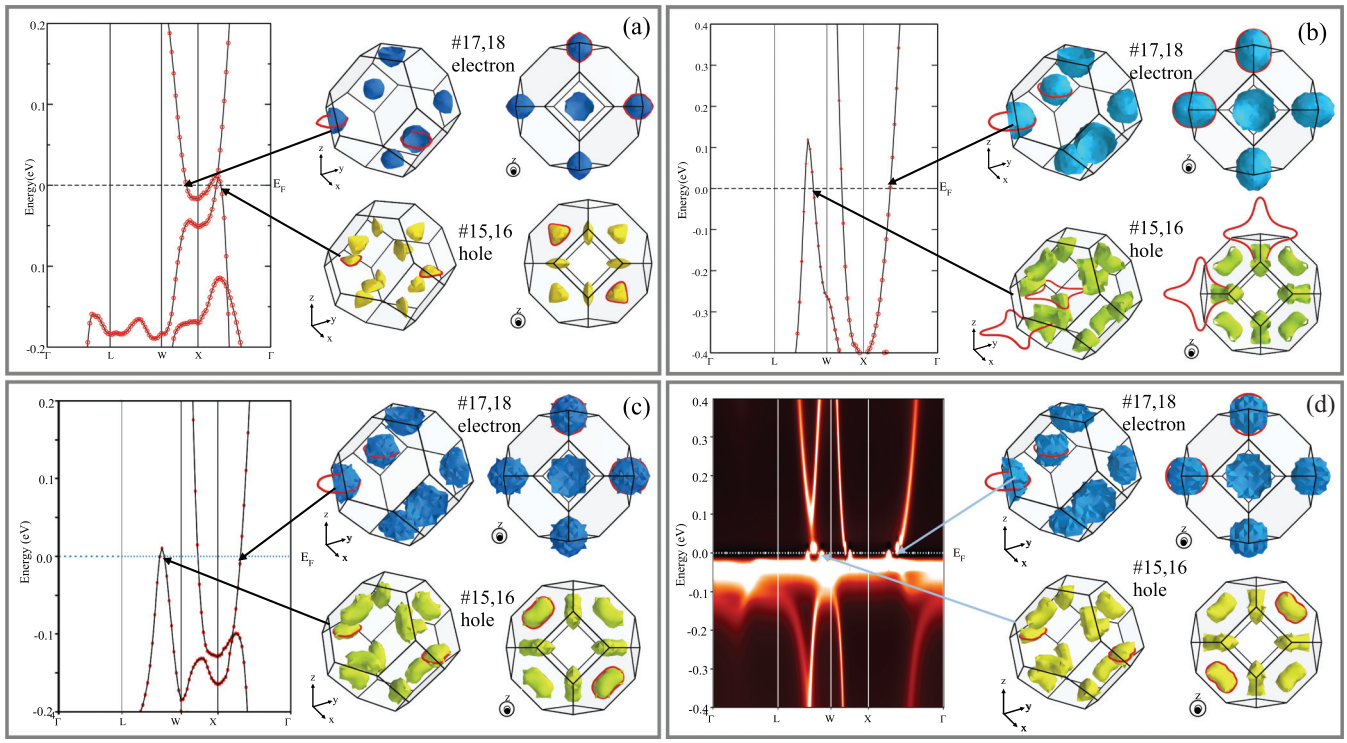

FIG. 3. The Fermi-surface topologies and corresponding closeup band dispersions for (a) the GGA method, (b) the GGA + U method, (c) the GGA + GutzA methods, and (d) the GGA + DMFT method. Each panel shows the hole (bands 15 and 16) and electron (bands 17 and 18) isosurfaces for two orientations as indicated by the coordinates to the bottom left of each BZ. The arrows from the Fermi surfaces to the band structures indicate the band intersections with the Fermi energy that correspond to each Fermi surface. Red lines are interposed on the Fermi surfaces to indicate the cross sections related to the dHvA extremal frequencies for an external **B** field parallel to the z-axis (**B** $\parallel z$). The path the band dispersions take through the BZ is shown in Fig. 2.

of the angular dependence on the dHvA frequencies and cyclotron masses is available in the SM document [43].

The most apparent development due to correlation effects is the expansion of both the electron and the hole Fermi surfaces. This can be seen in the increase in the dHvA frequencies, but expansion is clearest in the reciprocal volumes given in Table I. Compared to the GGA method, the GGA + U, GGA + GutzA, and GGA + DMFT reciprocal volumes increase by between 200% and 230% with the largest increase occurring between the GGA and the GGA + U methods. The nature of this volume expansion is consistent with the Luttinger theorem [48], which requires that the number of electrons be conserved and is directly proportional to the volume of the Fermi surface. Given that there are four bands (two degenerate pairs: 15 and 16 and 17 and 18) intersecting with the Fermi energy and assuming the lower-energy valence bands do not interact as the electron pocket increases in volume, the hole pocket must increase to compensate thereby conserving the total electron number, which leads to the simultaneous expansion of the Fermi surfaces of both the hole and the electron bands. This observation of Fermi pocket expansion is striking and unique for our multiband system, given that the strong-correlation effect does not change the Fermi-surface topology in a single-band-correlated electron model [48].

Because δ-Pu is a multi-f-orbital and a multi-f-electron electron system, the Pu 5f-orbital electrons are hybridized with the itinerant conduction electrons (mainly 6d-orbital electrons). The correlation effects narrow the effective f-electron band, and the 5f-band spectral weight is pushed away from the Fermi energy. A similar phenomenon is also noted in a more recent DFT + DMFT simulation on a uranium compound [49]. Our observation of Fermi-surface expansion with compensated electron and hole pockets comes from the fact that all 14 Pu-5f orbitals are hybridized mainly with the two Pu-6d_{z^2} and Pu-6d_{xy} orbitals in the energy range from -1.5 to 1.5 eV (Fig. 1). Because of the Pu-5f electron occupancy and strong spin-orbital coupling, the Fermi surface is mainly composed of the six spin orbitals belonging to the $j = 5/2$ subshell. The electronic correlations reduce the effective hybridization of the 5f electrons with the 6d-orbital conduction electrons. This reduction in hybridization adjusts the band energy dispersion around the Fermi energy in the Brillouin zone. In some regions (i.e., along the L-W segment of the k path), the dispersive 6d character is noticeably restored, causing the band bending up through the Fermi energy to form a hole pocket. Then, the electron band cutting the Fermi level around the X point should sink down to ensure the Luttinger sum rule requiring the expansion of then compensated Fermi pockets.

We have also analyzed the cyclotron effective masses on the Fermi surface. Their relationship to the dHvA cross section can be expressed as $m^* = \frac{\hbar^2}{2\pi e}\frac{\partial A}{\partial E}|_{E=E_F}$, which is in units of the electron mass m_e. The results of these calculations are recorded in Table I. They show a decrease in the effective

mass for methods including electronic correlations. As the cyclotron mass is calculated directly at the Fermi energy, we can explain the decrease in effective mass as stemming from the conspiring Fermi-surface expansion and band renormalization. Because the effective mass is inversely proportional to the slope of the energy band, a steeper band intersecting the Fermi energy leads to a smaller cyclotron mass. From the sections of the electronic band structures shown in Fig. 3, it is apparent that the slope of the hole and electron bands increases when moving from the GGA to the other strongly correlated electron methods. The electron bands (Nos. 17 and 18) calculated using the GGA + U have the steepest slope and, consequently, the most reduced effective mass. Similarly, the band structures from the GGA + GutzA and GGA + DMFT show bands of increased slope at the Fermi energy resulting in smaller effective masses.

C. Mass enhancement

Due to the multiband nature of the electronic structure in δ-Pu, the cyclotron mass is not an effective comparison of mass enhancement due to the overall correlation induced renormalization. Although the total number of electrons is conserved within each calculation method, the electron and holelike Fermi pockets expand when correlation effects are introduced, so in order to perform a meaningful comparison of the effective masses, a thermodynamic analysis of correlation induced self-energies of Pu-5f electrons is required [50]. This is beyond the GGA and GGA + U methods, which are limited to the single-particle Kohn-Sham formalism. We have performed the comparison for the GGA + GutzA and GGA + DMFT methods using

$$\frac{m^*_{qp}}{m_b} = \frac{\tilde{\rho}(E_F)}{\rho_b(E_F)}, \tag{3}$$

where $\rho_b(E_F) = \sum_j w_j \rho_{b,j}(E_F)$ is the band DOS and $\tilde{\rho}(E_F) = \sum_j w_j \rho_{b,j}(E_F)/z_j$ is the quasiparticle DOS. The partial density of states $\rho_{b,j}(E_F)$ is from the 14 5f-electron spin orbitals, and indices b and j are the band index and spin quantum number, respectively. In the case of the 5f electrons, j is either 5/2 or 7/2 where w_j is the number of electrons with either spin (six of $j = 5/2$ and eight of $j = 7/2$). In the GGA + DMFT method, the quasiparticle weight is $z_j = [1 - \partial\, \mathrm{Im}\, \Sigma_j(\omega_n)/\partial\omega_n|_{\omega_n \to 0}]^{-1}$, where $\mathrm{Im}\, \Sigma_j(\omega_n)$ is the imaginary part of the electronic self-energy in terms of the Matsubara frequency ω_n [45,51]. In the GGA + GutzA method, the quasiparticle weights are the elements z_j of the matrix $Z_j \equiv R_j^\dagger R_j$ where the matrix R_j is defined from the formulation of the rationally invariant slave boson theory derived by Lanatà *et al.* [30]. We estimate the effective mass for the GGA + GutzA calculation to be $m^*_{qp} = 1.30 m_b$ and $m^*_{qp} = 5.04 m_b$ for the GGA + DMFT calculation. This is consistent with correlation induced band renormalization theory [52,53], which finds that effective mass is enhanced, overall, by strongly correlated electron-electron interactions.

D. Temperature effects

We have also explored the temperature dependence of the Fermi-surface topology and electronic structure by using the GGA + DMFT method. Table II contains the dHvA results obtained from electronic structure data for three temperatures. As the temperature increased from 0 to 116 K, the extremal frequency of the hole bands (Nos. 15 and 16) decreased and that of the electron bands increased. From 116 to 1160 K, the band structure evolves significantly such that only two degenerate bands (Nos. 17 and 18) intersect the Fermi energy. The extremal frequency from this electron band isosurface is dramatically increased as is its reciprocal volume contained by the Fermi surface. It is noteworthy that the temperature $T = 1160$ K is well above the melting point for Pu. These results are intended to demonstrate the range of the GGA + DMFT capabilities as well as explore the band renormalization in the region where Pu 5f electrons become localized. Details of the electronic structure and Fermi-surface topology at $T = 1160$ K can be found in the SM document (Fig. S8) [43].

TABLE II. The dHvA and volume data for Fermi-surface calculations at temperatures up to 1160 K. Frequencies in kT, effective masses in units of m_e, and reciprocal Fermi-surface volumes in units of Å^{-3} are shown for the GGA + DMFT calculations of δ-Pu performed at $T = 116$ and $T = 1160$ K. These are compared to the extrapolated DMFT calculations for $T = 0$ K.

	$T = 0$ K			$T = 116$ K			$T = 1160$ K		
Band	f	m^*	V_{FS}	f	m^*	V_{FS}	f	m^*	V_{FS}
15 and 16	3.07	1.84	0.95	2.38	1.56	0.57			
17 and 18	6.18	2.17	0.95	7.02	1.98	1.14	13.80	2.36	3.04

IV. CONCLUDING DISCUSSION

In this paper, we provide detailed calculations of the Fermi-surface and associated mass renormalizations of δ-Pu. By using a comparison between the results of four different theoretical methods, we have found a significant impact of strong electronic correlations on the δ-Pu Fermi surface. For example, using a conventional GGA band-structure method as our starting point, three other methods that include electronic correlation effects beyond the GGA showed a Fermi-surface volume increase between 200 and 230% on individual Fermi pockets, depending on the method. The correlated-electron formalisms GGA + GutzA and GGA + DMFT, which take quantum entanglements in the electronic structure into account, were in relatively good agreement with each other with both providing a renormalized electronic band structure and enhanced effective masses. Given the similarity in the results between the two methods and the computational efficiencies present in the GGA + GutzA method, this suggests that the GGA + GutzA may be highly beneficial for future studies of Fermi-surface properties in other more complex Pu allotropes and alloys that may be beyond the current computational capabilities of the GGA + DMFT.

We also found that each theoretical method has a unique and identifiable impact on the electronic structure of δ-Pu. These differences in the nonmagnetic and paramagnetic Fermi-surface topologies, along with the Fermi-surface data calculated for the ferromagnetic and antiferromagnetic cases

(see the SM document [43]), should provide useful theoretical input to help analyze ongoing magnetic quantum oscillation measurements. These can be directly compared to our dHvA simulations by matching the frequency vs magnetic-field angle curves to experimental measurements performed on powder δ-Pu samples.

Additional analysis of the Coulomb interaction strength has been included in the SM documentation [43]. A study of increasing U using the GGA + U and GGA + GutzA was performed to explore the evolution of the electronic structure and Fermi surface (SM Figs. S4–S7) [43]. Figure S6 of the SM [43], in particular, shows very little change in the band structure between $U = 1$ and $U = 4.5$ eV. The most significant change occurs between $U = 0$ and $U = 1$ eV, suggesting that the introduction of electronic correlation effects has a more significant impact on the calculation than the strength of the interactions. Temperature effects for which there have been only a few extremely limited studies for Pu so far [4,54] are another interesting factor to influence the Fermi-surface topologies. Our comparison of calculations at 116 and 1160 K show a dramatic evolution of the electronic structure and, consequently, the Fermi surface. Further studies on the temperature dependence of electronic correlation effects will be beneficial in advancing our understanding of Pu and other actinides.

ACKNOWLEDGMENTS

We thank F. Ronning, Q. Si, J. Singleton, P. Wolfle, N. Harrison, J. M. Wills, and G. Zwicknagl for helpful discussions. This work was carried out under the auspices of the U.S. Department of Energy (DOE) National Nuclear Security Administration under Contract No. 89233218CNA000001. The Fermi-surface topology analysis work was supported by the LANL LDRD Program. The DFT + DMFT simulation work at high temperatures was supported by the NNSA Advanced Simulation and Computing Program. It was, in part, supported by the Center for Integrated Nanotechnologies, a DOE BES user facility, in partnership with the LANL Institutional Computing Program for computational resource.

[1] P. Weinberger, A. Gonis, A. Freeman, and A. Boring, Physica B+C **130**, 13 (1985).
[2] S. Y. Savrasov, G. Kotliar, and E. Abrahams, Nature (London) **410**, 793 (2001).
[3] J. Terry, R. Schulze, J. Farr, T. Zocco, K. Heinzelman, E. Rotenberg, D. Shuh, G. V. der Laan, D. Arena, and J. Tobin, Surf. Sci. **499**, L141 (2002).
[4] X. Dai, S. Y. Savrasov, G. Kotliar, A. Migliori, H. Ledbetter, and E. Abrahams, Science **300**, 953 (2003).
[5] G. Kotliar, S. Y. Savrasov, K. Haule, V. S. Oudovenko, O. Parcollet, and C. A. Marianetti, Rev. Mod. Phys. **78**, 865 (2006).
[6] P. Söderlind, F. Zhou, A. Landa, and J. E. Klepeis, Sci. Rep. **5**, 15958 (2015).
[7] J.-X. Zhu, R. C. Albers, K. Haule, G. Kotliar, and J. M. Wills, Nat. Commun. **4**, 2644 EP (2013).
[8] P. Söderlind, A. Landa, and B. Sadigh, Adv. Phys. **68**, 1 (2019).
[9] W. H. Brito and G. Kotliar, Phys. Rev. B **99**, 125113 (2019).
[10] S. Méot-Reymond and J. Fournier, J. Alloys Compd. **232**, 119 (1996).
[11] J.-X. Zhu, P. H. Tobash, E. D. Bauer, F. Ronning, B. L. Scott, K. Haule, G. Kotliar, R. C. Albers, and J. M. Wills, Europhys. Lett. **97**, 57001 (2012).
[12] M. Janoschek, P. Das, B. Chakrabarti, D. L. Abernathy, M. D. Lumsden, J. M. Lawrence, J. D. Thompson, G. H. Lander, J. N. Mitchell, S. Richmond, M. Ramos, F. Trouw, J.-X. Zhu, K. Haule, G. Kotliar, and E. D. Bauer, Sci. Adv. **1**, e1500188 (2015).
[13] R. Heffner, G. Morris, M. Fluss, B. Chung, D. MacLaughlin, L. Shu, and J. Anderson, Physica B **374-375**, 163 (2006).
[14] J. C. Lashley, A. Lawson, R. J. McQueeney, and G. H. Lander, Phys. Rev. B **72**, 054416 (2005).
[15] M. Janoschek, G. Lander, J. M. Lawrence, E. D. Bauer, J. C. Lashley, M. Lumsden, D. L. Abernathy, and J. D. Thompson, Proc. Natl. Acad. Sci. USA **114**, E268 (2017).
[16] A. Migliori, P. Söderlind, A. Landa, F. J. Freibert, B. Maiorov, B. J. Ramshaw, and J. B. Betts, Proc. Natl. Acad. Sci. USA **114**, E269 (2017).
[17] I. V. Solovyev, A. I. Liechtenstein, V. A. Gubanov, V. P. Antropov, and O. K. Andersen, Phys. Rev. B **43**, 14414 (1991).
[18] P. Söderlind, O. Eriksson, B. Johansson, and J. M. Wills, Phys. Rev. B **50**, 7291 (1994).
[19] J. Bouchet, B. Siberchicot, F. Jollet, and A. Pasturel, J. Phys.: Condens. Matter **12**, 1723 (2000).
[20] S. Y. Savrasov and G. Kotliar, Phys. Rev. Lett. **84**, 3670 (2000).
[21] P. Söderlind, Europhys. Lett. **55**, 525 (2001).
[22] P. Söderlind, A. Landa, and B. Sadigh, Phys. Rev. B **66**, 205109 (2002).
[23] A. L. Kutepov and S. G. Kutepova, J. Phys.: Condens. Matter **15**, 2607 (2003).
[24] B. Amadon and B. Dorado, J. Phys.: Condens. Matter **30**, 405603 (2018).
[25] B. Amadon, F. Jollet, and M. Torrent, Phys. Rev. B **77**, 155104 (2008).
[26] J.-X. Zhu, A. K. McMahan, M. D. Jones, T. Durakiewicz, J. J. Joyce, J. M. Wills, and R. C. Albers, Phys. Rev. B **76**, 245118 (2007).
[27] J. H. Shim, K. Haule, and G. Kotliar, Nature (London) **446**, 513 (2007).
[28] M. C. Gutzwiller, Phys. Rev. **137**, A1726 (1965).
[29] N. Lanatà, Y. Yao, C.-Z. Wang, K.-M. Ho, and G. Kotliar, Phys. Rev. X **5**, 011008 (2015).
[30] N. Lanatà, Y. Yao, X. Deng, V. Dobrosavljević, and G. Kotliar, Phys. Rev. Lett. **118**, 126401 (2017).
[31] J.-P. Julien and J. Bouchet, "Ab-initio gutzwiller method: First application to plutonium", *Recent Advances in the Theory of Chemical and Physical Systems* (Springer, Dordrecht, 2006), pp. 509–534.
[32] A. M. N. Niklasson, J. M. Wills, M. I. Katsnelson, I. A. Abrikosov, O. Eriksson, and B. Johansson, Phys. Rev. B **67**, 235105 (2003).
[33] M. D. Jones, J. C. Boettger, R. C. Albers, and D. J. Singh, Phys. Rev. B **61**, 4644 (2000).
[34] L. Nordström, J. M. Wills, P. H. Andersson, P. Söderlind, and O. Eriksson, Phys. Rev. B **63**, 035103 (2000).

[35] J. M. Wills, O. Eriksson, A. Delin, P. H. Andersson, J. J. Joyce, T. Durakiewicz, M. T. Butterfield, L. A. Morales, D. P. Moore, and A. J Arko, arXiv:cond-mat/0307767.
[36] X. Wu and A. K. Ray, Phys. Rev. B **72**, 045115 (2005).
[37] P. Söderlind, Phys. Rev. B **77**, 085101 (2008).
[38] D. Shoenberg, Proc. R. Soc. London, Ser. A **379**, 1 (1982).
[39] P. Rourke and S. Julian, Comput. Phys. Commun. **183**, 324 (2012).
[40] C.-C. Joseph Wang, M. D. Jones, and J.-X. Zhu, Phys. Rev. B **88**, 125106 (2013).
[41] P. Blaha, K. Schwarz, G. K. H. Madsen, D. Kvasnicka, and J. Luitz, *WIEN2K, An Augmented Plane Wave + Local Orbitals Program for Calculating Crystal Properties* (Karlheinz Schwarz, Technical Universität Wien, Austria, 2001).
[42] F. Ellinger, JOM **8**, 1256 (1956).
[43] See Supplemental Material at http://link.aps.org/supplemental/10.1103/PhysRevB.101.245156 for additional calculations and analyses.
[44] K. Haule, C.-H. Yee, and K. Kim, Phys. Rev. B **81**, 195107 (2010).
[45] J.-X. Zhu, M. Janoschek, R. Rosenberg, F. Ronning, J. D. Thompson, M. A. Torrez, E. D. Bauer, and C. D. Batista, Phys. Rev. X **4**, 021027 (2014).
[46] R. D. Cowan, *Theory of Atomic Structure and Spectra* (University of California Press, Oakland, CA, 1981).
[47] L. Jiao, Y. Chen, Y. Kohama, D. Graf, E. D. Bauer, J. Singleton, J.-X. Zhu, Z. Weng, G. Pang, T. Shang, J. Zhang, H.-O. Lee, T. Park, M. Jaime, J. D. Thompson, F. Steglich, Q. Si, and H. Q. Yuan, Proc. Natl. Acad. Sci. USA **112**, 673 (2015).
[48] A. C. Hewson, "Strongly correlated fermions", *The Kondo Problem to Heavy Fermions*, Cambridge Studies in Magnetism (Cambridge University Press, Cambridge, UK, 1993), pp. 313–362.
[49] Y. Xu, Y. Sheng, and Y.-f. Yang, Phys. Rev. Lett. **123**, 217002 (2019).
[50] K. Kanki and K. Yamada, J. Phys. Soc. Jpn. **66**, 1103 (1997).
[51] J.-X. Zhu, M. Janoschek, D. S. Chaves, J. C. Cezar, T. Durakiewicz, F. Ronning, Y. Sassa, M. Mansson, B. L. Scott, N. Wakeham, E. D. Bauer, and J. D. Thompson, Phys. Rev. B **93**, 144404 (2016).
[52] G. Zwicknagl and U. Pulst, Physica B **186-188**, 895 (1993).
[53] G. Zwicknagl, Rep. Prog. Phys. **79**, 124501 (2016).
[54] B. Dorado, F. Bottin, and J. Bouchet, Phys. Rev. B **95**, 104303 (2017).